ADVANCED ELECTRONIC MATERIALS
www.advelectronicmat.de

Complementary Organic Logic Gates on Plastic Formed by Self-Aligned Transistors with Gravure and Inkjet Printed Dielectric and Semiconductors

*Stuart G. Higgins, Beinn V. O. Muir, Giorgio Dell'Erba, Andrea Perinot, Mario Caironi, and Alasdair J. Campbell**

Organic electronics is a maturing field,[1] replete with a large variety of devices and fabrication technologies.[2] Often these are viewed in isolation, however ultimately it is likely that a holistic approach involving multiple techniques will yield the best manufacturing results. This will use the particular advantages of each technology and apply it where best-suited.[3]

As attention shifts to implementing complex circuit components, there is increasing focus on the use of complementary circuits. Complementary logic combines both p- and n-type semiconductors to yield circuits with better noise tolerance and lower power consumption,[4,5] although at expense of fabrication complexity (two semiconductors need to be deposited rather than one). This is where additive printing processes have the potential to yield dividends, allowing the selective deposition of materials onto the substrate. Among these techniques both inkjet and gravure printing have been widely adopted.

Inkjet printing has been used to fabricate a wide range of electrical components, including: complementary and ambipolar inverters,[6,7] quasistatic memory,[8] biosensors,[9] and organic photo detectors.[10] Similarly gravure printing has been used to fabricate circuits such as: complementary ring oscillators,[11] logic gates,[12] unipolar flip-flops and half-adders.[13,14] Although previous reports have combined gravure and inkjet printing to fabricate p-type organic field-effect transistors (OFETs),[15] there is a lack of direct comparative studies of the impact of each process on the electrical performance of devices. Here, we explore gravure versus inkjet printing of semiconductors, gravure printing versus photolithographic patterning of the OFET dielectric, and long-channel (>1 µm) versus short channel (<1 µm) OFETs.

Gravure printing enables very large-area, fast, roll-to-roll manufacturing, limited by the expense and time cost of fabricating clichés (printing plates).[16,17] Inkjet printing enables a computer-designed circuit to be printed readily and easily, limited by the relative throughput and speed of printing.[2] However, the resolution of both technologies is still restricted to the micrometer scale and larger by the challenge of reliably transferring inks onto a substrate without spreading or dewetting, while still maintaining electrical performance. While recent approaches are improving upon this limit, for example, the work of Kang et al. on gravure printed sub-5 µm gate electrodes,[18] or that of Sekitani et al. on 2 µm inkjet printed electrodes,[19] the options for patterning sub-micrometer electrode geometries are limited.

We have previously demonstrated how ultraviolet nanoimprint lithography (UV-NIL) is a viable method for patterning sub-micrometer channel length OFETs on plastic.[20] Our approach also uses self-aligned lithography to minimize the overlap between the gate–source and gate–drain electrodes, reducing parasitic overlap capacitances that reduce the switching speed of OFETs.[21,22] Self-alignment yields other benefits such as overcoming equipment alignment tolerances, reducing leakage currents, and is compatible with more complex circuitry such as self-aligned unipolar ring oscillators.[23] In this work, we have used bottom-gate bottom-contact architectures, to avoid exposing the semiconductor to both the ultraviolet light and processing chemicals used for self-alignment. In addition to self-alignment, here we extend the fabrication approach further by incorporating gravure printed dielectrics and semiconductors, as well as inkjet printed semiconductors. We demonstrate both p- and n-type devices patterned side-by-side on the same substrate along with complementary inverters and logic gates.

Figure 1 illustrates the materials and architectures used in this work. Aluminum OFET gates were patterned either photolithographically (PL) or via UV-NIL. A cross-linkable proprietary dielectric (GSID 938109-1, BASF)[24,25] was either PL patterned or gravure printed. Self-aligned gold electrodes were patterned

Dr. S. G. Higgins,[+] Dr. B. V. O. Muir, Dr. A. J. Campbell
Department of Physics and the Centre for Plastic Electronics
Imperial College London
South Kensington Campus
London SW7 2AZ, UK
E-mail: alasdair.campbell@imperial.ac.uk

Dr. B. V. O. Muir
Department of Chemistry and the Centre for Plastic Electronics
Imperial College London
South Kensington Campus
London SW7 2AZ, UK

G. Dell'Erba, A. Perinot, Dr. M. Caironi
Centre for Nano Science and Technology @ PoliMi
Istituto Italiano di Tecnologia
Via Pascoli 70/3, 20133 Milano, Italy

G. Dell'Erba
Dipartimento di Elettronica
Informazione e Bioingegneria
Politecnico di Milano
Piazza Leonardo da Vinci, 32
20133, Milano Italy

[+]Present address: Cavendish Laboratory, University of Cambridge, Cambridge CB3 0HE, UK

This is an open access article under the terms of the Creative Commons Attribution License, which permits use, distribution and reproduction in any medium, provided the original work is properly cited.

The copyright line of this paper was changed 10 August 2016 after initial publication.

DOI: 10.1002/aelm.201500272

 © 2016 The Authors. Published by WILEY-VCH Verlag GmbH & Co. KGaA, Weinheim

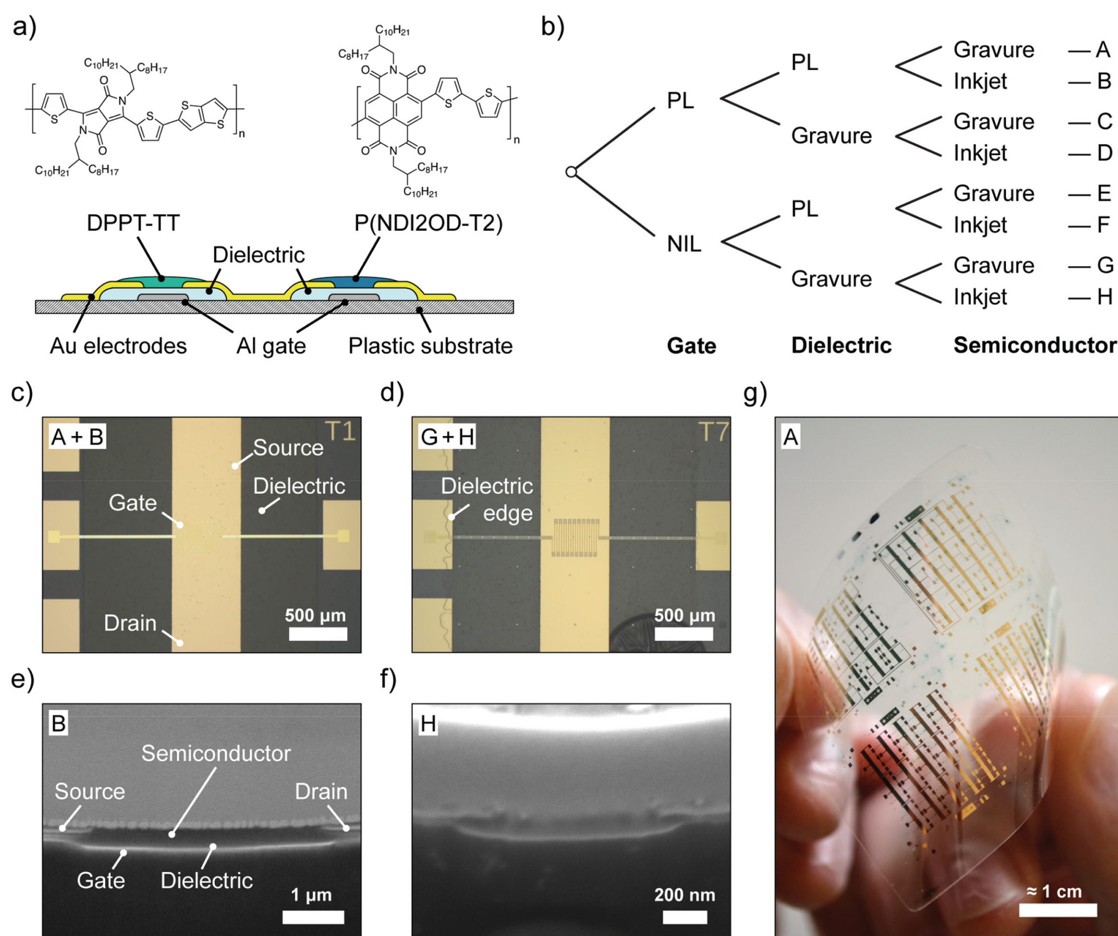

Figure 1. a) Device architecture and chemical structures of DPPT-TT and P(NDI2OD-T2). b) Tree diagram of architecture variants and identifying letters. Optical micrographs of c) PL patterned variants A & B and d) NIL/gravure variants G & H prior to semiconductor deposition. Note 'T1' and 'T7' are identifiers patterned on the substrate and should not be confused with annotations in white boxes. e,f) SEM images of cross-section through equivalent devices. Note both gold and platinum have been deposited on top of the device architecture as part of FIB–SEM process. g) Photograph of a finished flexible substrate (50 × 50 mm^2) showing OFETs, inverters and complementary logic circuits.

via a bilayer liftoff process, before semiconductor patterning by either gravure or inkjet printing. Each substrate variant had two different semiconductors patterned on adjacent devices to facilitate complementary circuits. We chose two high performance polymeric semiconductors, based on previous demonstrations of transistor performance and printability.[2,8,26] These were the predominantly p-type polymer diketopyrrolopyrrole-thieno[3,2-*b*]thiophene (DPPT-TT);[27] and the n-type poly([*N,N′*-bis(2-octyldodecyl)-naphthalene-1,4,5,8-bis(dicarboximide)-2,6-diyl]-alt-5,5′-(2,2′-bithiophene)) (P(NDI2OD-T2)) (structures in Figure 1a).[28] All devices are bottom-gate bottom-contact as necessitated by our self-aligned approach. The fabrication process is discussed in detail in the Supporting Information and also in our previous work.[20]

Figure 1c–f) show the predominantly PL patterned (variants A + B) and printed (variants G + H) devices. The edges of the dielectric square are just visible in the optical micrographs (Figure 1c,d). The relatively large size of the dielectric region is to compensate for a nominal alignment tolerance of ±0.5 mm in the gravure printer. These dimensions can be readily downscaled using a gravure printer featuring an alignment tool. We observed that gravure printing the dielectric yields a larger line-edge roughness compared to photopatterning. This rippling of the printed edge is common throughout gravure printing, emerging from a combination of hydrodynamic instability in ink during the printing process,[29] and as a consequence of the underlying cliché cell structure.[30] Surface profilometry measurements indicated a slight 'coffee ring effect' at the edge of the gravure printed structure,[31] but an otherwise homogenous flat film in the device region. Although based on the same dielectric, the gravure printed ink formulation yielded a thinner dielectric layer (86 ± 14 nm) compared to the PL patterned layer (174 ± 26 nm) (see Figure S1 in the Supporting Information).

We used a meandering gate to give self-aligned interdigitated source–drain fingers with a nominal channel width of W = 5000 µm and length of L = 3 µm and L = 0.9 µm for PL and NIL patterned gates, respectively. Focussed-ion beam scanning electron microscopy (FIB-SEM) was used to verify the nanoscale structure of the devices, as shown in Figure 1e,f. Substrates were milled by irradiation with gallium ions, before imaging the device cross-section using SEM. Exceptionally low gate–drain and gate–source electrode overlaps of ≤210 nm were observed. By comparison, conventionally aligned common-gate

© 2016 The Authors. Published by WILEY-VCH Verlag GmbH & Co. KGaA, Weinheim

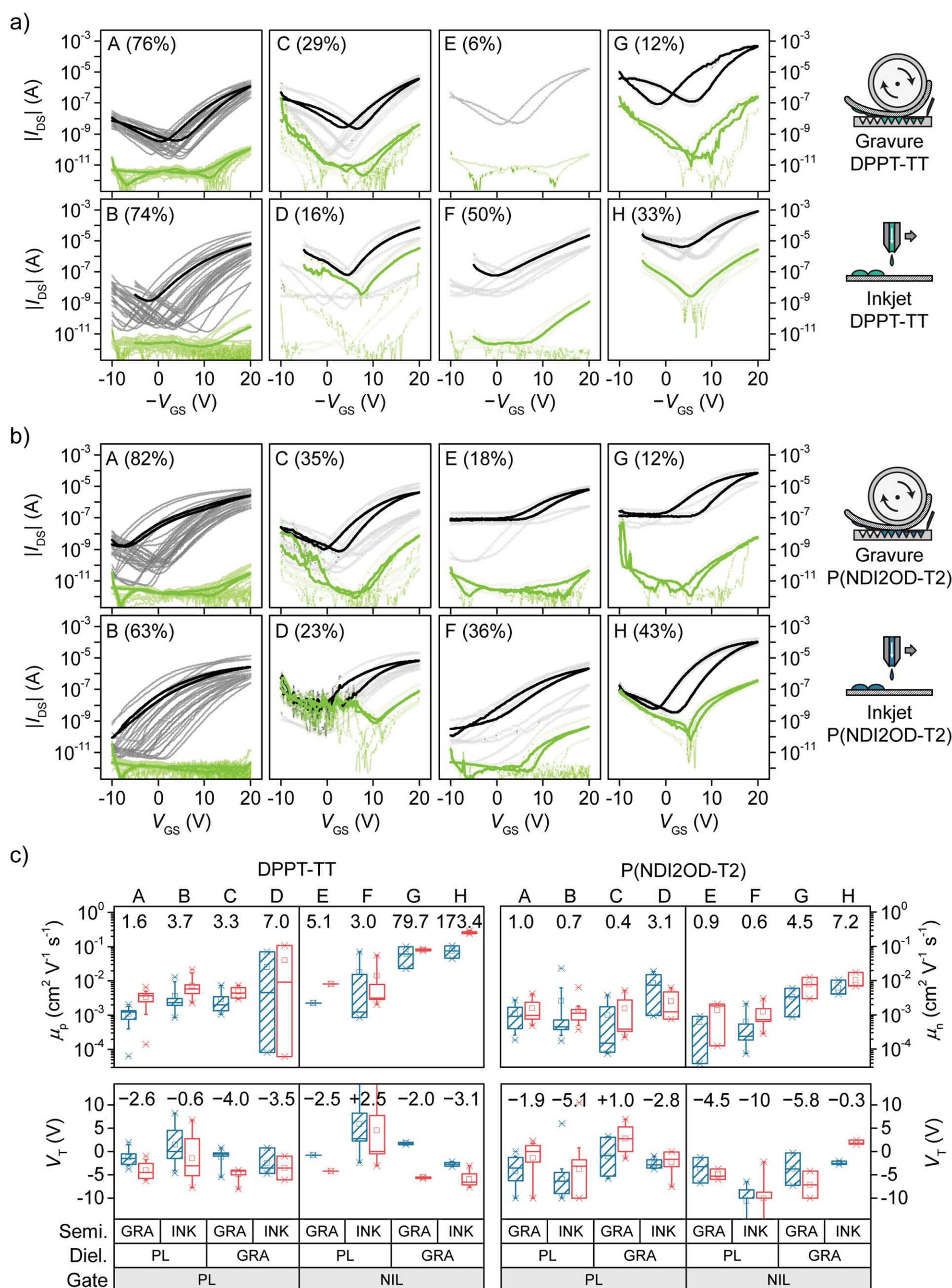

Figure 2. OFET transfer characteristics for a) p-type and b) n-type devices measured at $|V_{DS}| = 20$ V, with gate current flow (I_{GS}) in green. Bold traces represent mean characteristics of all devices in that plot; percentages indicate test yield. Note all scales are equal and p-type data is plotted against $-V_{GS}$ to allow direct comparison with n-type. c) Box plots summarising extracted figures-of-merit for forward (teal, hatched) and reverse (red, unhatched) transfer sweeps. Boxes represent 25th and 75th percentiles, horizontal lines in boxes the median, squares (□) the mean, whiskers (–) the 10th and 90th percentiles and crosses (×) the minimum and maximum values obtained. The median mobility (specified as $\times 10^{-3}$ cm^2 V^{-1} s^{-1}) and threshold voltage (V) of both forward and backward sweeps is quoted explicitly adjacent to each pair of boxes.

devices typically have overlaps on the order of many hundreds of micrometers. We also used the SEM images and image analysis software to calculate the effective channel length of each variant.[32] NIL patterned channels were found to be slightly smaller and PL patterned channels slightly larger than the nominal L values (see Table S1 in the Supporting Information for values).

Figure 2 summarizes the OFET device data. The transfer characteristics of each architecture variant for p- and n-type OFETs are shown in Figure 2a,b, respectively, along with box plots of the extracted figures of merit in Figure 2c. Examples of the output and transfer characteristics for best performing 'hero' devices are shown in the Supporting Information (Figure S2).

© 2016 The Authors. Published by WILEY-VCH Verlag GmbH & Co. KGaA, Weinheim

In the case of photopatterned dielectrics (variants A + B, E + F) exceptionally low leakage currents of <0.1 nA are observed, another advantage of self-aligned architectures.[22] Gravure printed dielectric (variants C + D, G + H) exhibit slightly greater leakage as a result of the ≈50% thinner layer deposited by printing (as discussed above). Despite this the relative ratio of drain to gate current remains in the range 10^2–10^4 for these devices, yielding functioning OFETs and circuits.

From Figure 2 we note that the combination of sub-micrometer NIL-patterned channels, thin gravure printed dielectric and inkjet printed semiconductor (variant H) yield both p- and n-type devices with the highest effective mobilities, with median values of μ_p = 0.173 cm^2 V^{-1} s^{-1} and μ_n = 0.007 cm^2 V^{-1} s^{-1}, respectively. Similarly, the best performing gravure printed semiconductor devices (variant G) exhibit median values of μ_p = 0.079 cm^2 V^{-1} s^{-1} and μ_n = 0.005 cm^2 V^{-1} s^{-1}, respectively. The observed boost for NIL patterned short channel devices suggests the onset of short-channel effects such as drain-induced barrier lowering,[5] which increase current flow through the device.[33]

It is interesting to note from Figure 2c that to within uncertainty there is no significant difference in the extracted mobility for devices with PL patterned gates (variants A–D) for both DPPT-TT and P(NDI2OD-T2) semiconductors, unlike for NIL patterned gates (variants E–H). This suggests that at larger channel lengths the effective mobility obtainable is relatively process agnostic, while at shorter channel lengths the choice of deposition method has a greater influence. For the bottom-gate bottom-contact OFETs used here, the differing drying dynamics of gravure (simultaneous patterning and solvent evaporation) and inkjet (sequential deposition and drying, combined with partial re-dissolution of the semiconductor by consecutive drops) may be responsible for the differences observed here.[16,31,34] However, ultimately for larger channel length devices (typical in most applications) it appears for this material system that there is no electrical significance to using either inkjet or gravure printing for semiconductor deposition. In this case other factors, such as process throughput or ability to rapidly modify the printed design, may favor one technique over the other.

Uniformity was found to be an issue for both gravure and inkjet printed semiconductors, irrespective of material. The spread of threshold voltages suggests this variation originates at the dielectric–semiconductor interface. Although we use a cross-linked dielectric system, a viscosity modifier (high molecular weight poly(methyl methacrylate) (PMMA)) also forms part of the ink formulation and remains in the layer after cross-linking. Disordered dipoles in PMMA dielectrics have previously been observed to cause energetic disorder at the dielectric–semiconductor interface, yielding variation in device characteristics.[35] This represents one of the challenges of printed approaches; for example, for gravure printing reducing the PMMA content impacts ink viscosity and hence film homogeneity.[36,37] Other methods for varying ink viscosity (concentration, long-chain solvent blends) are a possible approach to this issue.[29]

Process yield was predominantly dictated by two factors. In the case of gravure printed dielectric (variant C + D, G + H), the thinner layer combined with process variation increased the probability of breakdown pathways forming, as reflected in the higher leakage observed in functioning devices, which may be mitigated by increasing the layer thickness. For NIL patterned gates (E–H), the initial imprint step was significantly hindered by a lack of NIL tool, we instead relied on a customized mask aligner. While useful for proof-of-concept testing, the imprint step was found to trap air, displacing the resist during patterning and limiting yield at this early step in the processing. This is a well-understood phenomenon and has been engineered out of modern NIL tools.[38,39]

From our devices we were able to fabricate complementary inverters comprising DPPT-TT and P(NDI2OD-T2) OFETs to demonstrate the feasibility of complementary circuits, as shown in **Figure 3** (implementation shown in Figure S3 in the Supporting Information). Other than the examples described below, variants E to G yielded few functioning devices due to the low NIL gate yield, as discussed above. Figure 3a shows an example of the voltage transfer characteristics (VTCs) achieved by combining two NIL patterned gate devices (connected via external probing). By tuning the operating bias, highly abrupt switching behavior was observed at V_{dd} = +9 V with a peak gain of 28. The current into the p-type load transistor was sub-30 nA in both the static on- and off-states, a direct result of the low leakage behavior obtained using self-alignment. Repeat testing of the inverter at multiple operating biases confirmed stable behavior (Figure S4 in the Supporting Information shows stability, current, and inkjet printed variant measurements).

According to classical CMOS theory the switching threshold is a function of operating bias, device geometry, dielectric specific capacitance, and the threshold voltages of the constituent OFETs.[4,40] In the ideal case $V_{Th} = V_{dd}/2$, helping to maximize the circuit noise margins. Here deviations from the ideal case are expected as a direct result of using a balanced OFET geometry, hence the switching threshold is strongly dictated by the relative p- and n-type mobilities (μ_p and μ_n), and can be further improved by tailoring the channel dimensions accordingly.

From Figure 3b,c we note that inverters with inkjet printed semiconductor (variants B + D) gave the highest gains (median values of G = 8.0, G = 8.1, respectively), with a peak gain of G = 17.3 recorded. We also observe systematically lower switching thresholds for devices with gravure printed semiconductor (variants A + C) compared to inkjet printed (variants B + D). The origin of the shift is unclear, but is a consequence of the parameter spread observed in single OFET devices.

It is important to note the impact of the ambipolar behavior of both DPPT-TT and P(NDI2OD-T2), as observed in Figure 2 and in similar devices.[8] This, along with threshold voltage variation, can result in the P(NDI2OD-T2) OFET channel remaining partially conductive when the input is biased low, and vice versa for the DPPT-TT device. The consequence of this is a reduction in the output high (V_{OH}) and increased output low (V_{OL}) voltages, as seen in Figure 3. Output high and output low voltages represent the voltage appearing at V_{OUT} in both of the static inverter states. In the ideal case $V_{OH} = V_{dd}$, and V_{OL} = 0 V, representing full inversion between the power supply voltage and ground. One method for preventing ambipolar behavior is through solution-processed selective contact engineering.[41,42]

Finally, we fabricated complementary NAND and NOR logic gates as proof of concept for our technology. Figure 3d shows the response of both gravure and inkjet printed semiconductor NAND gates to an alternating stimulus. This plot shows two

© 2016 The Authors. Published by WILEY-VCH Verlag GmbH & Co. KGaA, Weinheim

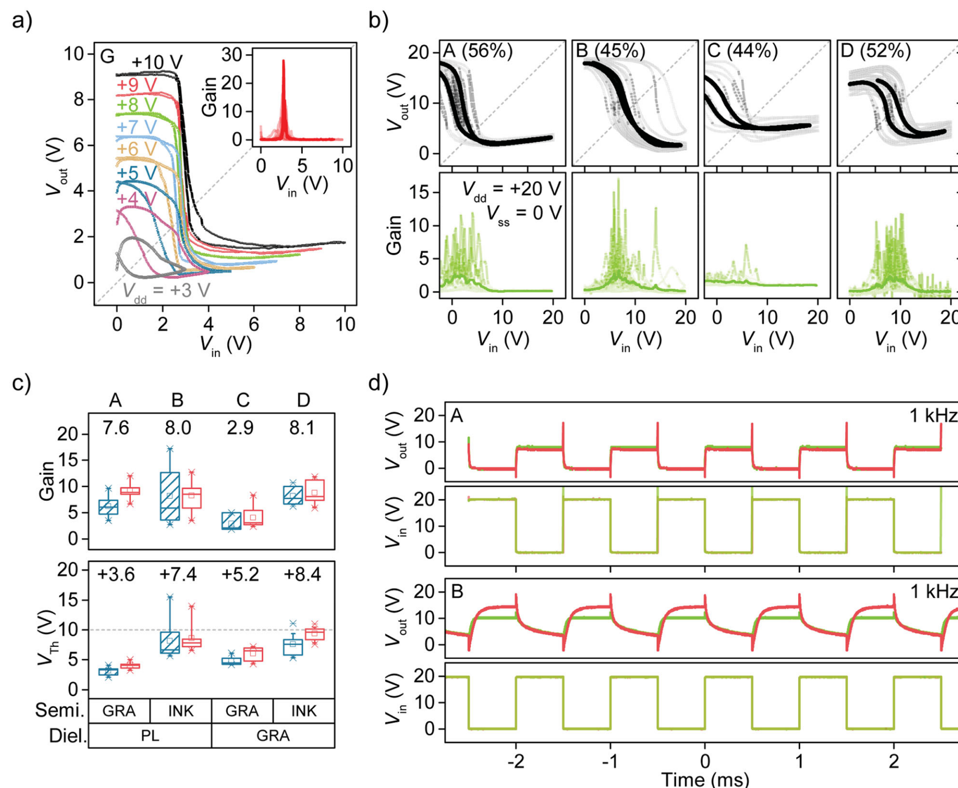

Figure 3. a) VTCs for a complementary inverter as a function of operating bias V_{dd}. Device comprises NIL patterned gate, gravure printed dielectric, and gravure printed p- and n-type semiconductors (variant G). Inset shows composite of corresponding gain characteristics. b) Composite of VTCs measured for A–D variants with corresponding gain curves. Bold traces represent mean characteristics of all devices in that plot. Dashed lines indicate $V_{in} = V_{out}$; percentages indicate test yield. c) Box plots of extracted gain and switching thresholds from b); dashed line indicates ideal switching threshold; box parameters as used in Figure 2. The median gain and switching threshold (V) of both forward and backward sweeps is quoted explicitly adjacent to each pair of boxes. d) Response of complementary NAND gates to alternating input for devices with gravure printed (variant A) and inkjet-printed (variant B) semiconductors; V_{dd} = +20 V.

overlapping measurements, in which one input is held high, and the other switched, e.g., A_{in} = +20 V and $B_{in} = +V_{in}$. The gate shows the expected response, with the output high when both inputs are low and vice versa. Given the symmetrical nature of the NAND and NOR gate implementation, we also fabricated a NOR logic gate (see Figures S5–S7 in the Supporting Information for implementations and NOR gate response).

In the ideal case the output voltage of each gate should be as close to the drive voltage as possible, i.e., $V_{out} \approx V_{dd}$. In this case we note that the output in both cases is capped at just below V_{out} = +10 V, and again this is as a result of deliberately using device geometries un-tuned to the specific characteristics of the semiconductor system. It is also noted that in Figure 3d the output voltage differs by approximately $V_{dd}/4$ depending on which input is performing the switching. This suggests slight variation in the two p-type OFETs that comprise the pull-up circuit. Despite this, these results demonstrate the feasibility of combining self-aligned OFETs on plastic to form functional complementary circuits.

In conclusion, we have shown how a holistic approach to device fabrication, combining the advantages of multiple technologies, can produce OFETs with enhanced electrical performance. For ≈3 µm channel length we observed no statistically significant difference between the use of photolithography or gravure printing for patterning the dielectric layer. Similarly, no difference was observed between inkjet or gravure printed semiconductors. However, this was not true for sub-micrometer devices, whereby the combination of gravure printed dielectric and inkjet printed semiconductor yielded higher effective mobilities. From these results we recommend that gravure printing is an excellent substitute for lithographically patterned dielectric, helping to contribute to improved device performance. Self-aligned devices serve not only as a method for beating equipment alignment tolerances and achieving nanoscale aligned device structures, but also yield excellent low leakage performance. As organic circuit design becomes increasingly complex inevitably focus will shift to the downscaling of channel lengths. These findings suggest that the differences in deposition methods will become more pronounced as a result; however, for large scale devices users should consider other factors, such as speed, practicality, and cost when considering which techniques to use.

Experimental Section

Full fabrication and characterization details are provided in the Supporting Information.

 © 2016 The Authors. Published by WILEY-VCH Verlag GmbH & Co. KGaA, Weinheim

Supporting Information

Supporting Information is available from the Wiley Online Library or from the author.

Acknowledgements

The authors acknowledge valuable support and discussion with Martin Heeney, Nikolay Vaklev, Caterina Ware, and members of the POLARIC consortium. This work was supported by the European Commission's 7th Framework Programme (FP7/2007-2013) under Grant Agreement No. 247978, 'Printable, Organic and Large-Area Realisation of Integrated Circuits' (POLARIC). S. G. Higgins was supported by the Engineering and Physical Sciences Research Council (EPSRC) under Grant No. EP/P505550/1. M. Caironi acknowledges the financial support of the European Research Council (ERC) under the European Union's Horizon 2020 research and innovation programme 'HEROIC', grant agreement 638059. Open data statement: the underlying data supporting this publication is available at: http://dx.doi.org/10.5281/zenodo.33112

Received: August 18, 2015
Revised: November 3, 2015
Published online: January 7, 2016

[1] H. Sirringhaus, *Adv. Mater.* **2014**, *26*, 1319.
[2] K.-J. Baeg, M. Caironi, Y.-Y. Noh, *Adv. Mater.* **2013**, *25*, 4210.
[3] L. Teng, M. Plötner, A. Türke, B. Adolphi, A. Finn, R. Kirchner, W.-J. Fischer, *Microelectron. Eng.* **2013**, *110*, 292.
[4] S. M. Kang, Y. Leblebici, *CMOS Digital Integrated Circuits: Analysis and Design*, McGraw-Hill, New York, NY, **1999**.
[5] S. M. Sze, K. K. Ng, *Physics of Semiconductor Devices*, John Wiley & Sons, Hoboken, NJ **2006**.
[6] W. Smaal, C. Kjellander, Y. Jeong, A. Tripathi, B. Van Der Putten, A. Facchetti, H. Yan, J. Quinn, J. Anthony, K. Myny, W. Dehaene, G. Gelinck, *Org. Electron.* **2012**, *13*, 1686.
[7] D. Khim, K.-J. Baeg, M. Kang, S.-H. Lee, N.-K. Kim, J. Kim, G.-W. Lee, C. Liu, D.-Y. Kim, Y.-Y. Noh, *ACS Appl. Mater. Interfaces* **2013**, *5*, 12579.
[8] S. Mandal, G. Dell'Erba, A. Luzio, S. G. Bucella, A. Perinot, A. Calloni, G. Berti, G. Bussetti, L. Duò, A. Facchetti, Y.-Y. Noh, M. Caironi, *Org. Electron.* **2015**, *20*, 132.
[9] M. Medina-Sánchez, C. Martínez-Domingo, E. Ramon, A. Merkoçi, *Adv. Funct. Mater.* **2014**, *24*, 6291.
[10] K.-J. Baeg, M. Binda, D. Natali, M. Caironi, Y.-Y. Noh, *Adv. Mater.* **2013**, *25*, 4267.
[11] H. Kempa, M. Hambsch, K. Reuter, M. Stanel, G. C. Schmidt, B. Meier, A. C. Hubler, *IEEE Trans. Electron Devices* **2011**, *58*, 2765.
[12] M. Hambsch, K. Reuter, H. Kempa, A. C. Hübler, *Org. Electron.* **2012**, *13*, 1989.
[13] J. Noh, V. Subramanian, *IEEE Electron Device Lett.* **2011**, *32*, 638.
[14] J. Noh, S. Kim, K. Jung, J. Kim, S. Cho, G. Cho, *IEEE Electron Device Lett.* **2011**, *32*, 1555.
[15] A. de la Fuente Vornbrock, D. Sung, H. Kang, R. Kitsomboonloha, V. Subramanian, *Org. Electron.* **2010**, *11*, 2037.
[16] M. M. Voigt, A. Guite, D.-Y. Chung, R. U. A. Khan, A. J. Campbell, D. D. C. Bradley, F. Meng, J. H. G. Steinke, S. Tierney, I. McCulloch, H. Penxten, L. Lutsen, O. Douheret, J. Manca, U. Brokmann, K. Sönnichsen, D. Hülsenberg, W. Bock, C. Barron, N. Blanckaert, S. Springer, J. Grupp, A. Mosley, *Adv. Funct. Mater.* **2010**, *20*, 239.
[17] H. Kipphan, *Handbook of Print Media*, Springer-Verlag, Heidelberg, Germany, **2001**.
[18] H. Kang, R. Kitsomboonloha, K. Ulmer, L. Stecker, G. Grau, J. Jang, V. Subramanian, *Org. Electron.* **2014**, *15*, 3639.
[19] T. Sekitani, Y. Noguchi, U. Zschieschang, H. Klauk, T. Someya, *Proc. Natl. Acad. Sci. USA* **2008**, *105*, 4976.
[20] S. G. Higgins, B. V. O. Muir, J. Wade, J. Chen, B. Striedinger, H. Gold, B. Stadlober, M. Caironi, J.-S. Kim, J. H. G. Steinke, A. J. Campbell, *Adv. Electron. Mater.* **2015**, *1*, 1500024.
[21] Y.-Y. Noh, N. Zhao, M. Caironi, H. Sirringhaus, *Nat. Nanotechnol.* **2007**, *2*, 784.
[22] U. Palfinger, C. Auner, H. Gold, A. Haase, J. Kraxner, T. Haber, M. Sezen, W. Grogger, G. Domann, G. Jakopic, J. R. Krenn, B. Stadlober, *Adv. Mater.* **2010**, *22*, 5115.
[23] H. Gold, A. Haase, A. Fian, C. Prietl, B. Striedinger, F. Zanella, N. Marjanović, R. Ferrini, J. Ring, K.-D. Lee, R. Jiawook, A. Drost, M. König, R. Müller, K. Myny, J. Genoe, U. Kleb, H. Hirshy, R. Prétôt, J. Kraxner, R. Schmied, B. Stadlober, *Org. Electron.* **2015**, *22*, 140.
[24] N. L. Vaklev, R. Müller, B. V. O. Muir, D. T. James, R. Pretot, P. van der Schaaf, J. Genoe, J.-S. Kim, J. H. G. Steinke, A. J. Campbell, *Adv. Mater. Interfaces* **2014**, *1*, 1300123.
[25] M. Kastler, S. Köhler, *WO 2010/136385 A1*, **2010**.
[26] S. Holliday, J. E. Donaghey, I. McCulloch, *Chem. Mater.* **2014**, *26*, 647.
[27] Z. Chen, M. J. Lee, R. Shahid Ashraf, Y. Gu, S. Albert-Seifried, M. Meedom Nielsen, B. Schroeder, T. D. Anthopoulos, M. Heeney, I. McCulloch, H. Sirringhaus, *Adv. Mater.* **2012**, *24*, 647.
[28] H. Yan, Z. Chen, Y. Zheng, C. Newman, J. R. Quinn, F. Dötz, M. Kastler, A. Facchetti, *Nature* **2009**, *457*, 679.
[29] G. Hernandez-Sosa, N. Bornemann, I. Ringle, M. Agari, E. Dörsam, N. Mechau, U. Lemmer, *Adv. Funct. Mater.* **2013**, *23*, 3164.
[30] S. G. Higgins, F. L. Boughey, R. Hills, J. H. G. Steinke, B. V. O. Muir, A. J. Campbell, *ACS Appl. Mater. Interfaces* **2015**, *7*, 5045.
[31] H. Kang, D. Soltman, V. Subramanian, *Langmuir* **2010**, *26*, 11568.
[32] C. A. Schneider, W. S. Rasband, K. W. Eliceiri, *Nat. Methods* **2012**, *9*, 671.
[33] J. Haddock, X. Zhang, S. Zheng, Q. Zhang, S. Marder, B. Kippelen, *Org. Electron.* **2006**, *7*, 45.
[34] D. Soltman, B. Smith, H. Kang, S. J. S. Morris, V. Subramanian, *Langmuir* **2010**, *26*, 15686.
[35] H. Sirringhaus, *Adv. Mater.* **2005**, *17*, 2411.
[36] D. Sung, A. de la Fuente Vornbrock, V. Subramanian, *IEEE Trans. Compon. Packag. Technol.* **2010**, *33*, 105.
[37] H. Kang, R. Kitsomboonloha, J. Jang, V. Subramanian, *Adv. Mater.* **2012**, *24*, 3065.
[38] L. J. Guo, *Adv. Mater.* **2007**, *19*, 495.
[39] R. Ji, M. Hornung, M. A. Verschuuren, R. van de Laar, J. van Eekelen, U. Plachetka, M. Moeller, C. Moormann, *Microelectron. Eng.* **2010**, *87*, 963.
[40] R. Jaeger, T. Blalock, *Microelectronics Circuit Design*, McGraw-Hill Higher Education, New York, NY, **2010**.
[41] D. Khim, K.-J. Baeg, M. Caironi, C. Liu, Y. Xu, D.-Y. Kim, Y.-Y. Noh, *Adv. Funct. Mater.* **2014**, *24*, 6252.
[42] K.-J. Baeg, J. Kim, D. Khim, M. Caironi, D.-Y. Kim, I.-K. You, J. R. Quinn, A. Facchetti, Y.-Y. Noh, *ACS Appl. Mater. Interfaces* **2011**, *3*, 3205.

 © 2016 The Authors. Published by WILEY-VCH Verlag GmbH & Co. KGaA, Weinheim